TISSUE ENGINEERING: Part A
Volume 20, Numbers 9 and 10, 2014

DOI: 10.1089/ten.tea.2013.0314

Long-Term Tracking of Segmental Bone Healing Mediated by Genetically Engineered Adipose-Derived Stem Cells: Focuses on Bone Remodeling and Potential Side Effects

Chin-Yu Lin, PhD,[1,*] Yu-Han Chang, MD, PhD,[2,3,*] Li-Yu Sung, MS,[1] Chiu-Ling Chen, MS,[1] Shih-Yeh Lin, PhD,[1] Kuei-Chang Li, MS,[1] Tzu-Chen Yen, MD, PhD,[2,4] Kun-Ju Lin, MD, PhD,[4,5] and Yu-Chen Hu, PhD[1]

We previously showed that transplantation of adipose-derived stem cells (ASCs) engineered with hybrid baculovirus (BV) persistently expressing bone morphogenetic protein 2 (BMP2)/vascular endothelial growth factor (VEGF) into segmental defects in New Zealand White (NZW) rabbits led to successful defect reunion. By using microcomputed tomography and histology, here we further demonstrated that transplanting the hybrid BV-engineered ASCs into the massive defects (10 mm in length) at the femoral diaphysis of NZW rabbits resulted in trabecular bone formation in the interior via endochondral ossification and bone remodeling at 3 months post-transplantation. The progression of bone remodeling gave rise to the resorption of trabecular bone and conspicuous reconstruction of medullary cavity and cortical bone with lamellar structure at 8 months post-transplantation, hence conferring mechanical properties that were comparable to those of nonoperated femora. Importantly, X-ray, positron emission tomography/computed tomography scans, and histopathology revealed no signs of heterotopic bone formation and tumor formation. These data altogether attested that the genetically engineered ASCs and prolonged BMP2/VEGF expression not only healed and remodeled the stringent segmental defects, but also revitalized the defects into living bone tissues that structurally and biomechanically resembled intact bones without appreciable side effects, making it one step closer to translate this technology to the clinical setting.

Introduction

HUMAN LONG BONES consist of two forms of bone tissue; cortical bone constitutes the outer wall to provide the major mechanical support and contains blood vessels, while cancellous bone consists of trabecular plates and bars that are found in the highly vascularized interior.[1] An adult long bone has a shaft (diaphysis) with two expanded ends and a large inner medullary cavity filled with bone marrow, fat tissue, and blood vessels. In the diaphysis, almost the entire thickness of bone tissue is cortical and only a small amount of trabecular bone lines the inner surface of cortical bone and faces the medullary cavity.[2] In general, healing of bone fractures involves (1) initial inflammation, (2) subsequent production of bone callus with poorly organized matrix for bony union, and (3) ensuing remodeling process that reshapes the bone tissues by removing, replacing, and reorganizing cells and matrix.[1] However, management of large segmental defects in the long bone following trauma or tumor resection still poses a tremendous challenge for orthopedic surgeons,[3] partly because the injury impairs blood supply and results in ischemia, osteonecrosis, bone loss, and ultimately nonunion.[1]

Facing these challenges, bone morphogenetic protein 2 (BMP2) was exploited to expedite and ameliorate the bone healing[4] and allogeneic bone graft impregnated with recombinant BMP2 (Infuse® Bone Graft/LT-Cage®; Medtronic) has been approved by the Food and Drug Administration for spinal fusion. However, the graft may not suffice to completely heal massive segmental defects in long bones. Other than BMP2, poor vascularization leads to suboptimal bone repair and vascular endothelial growth

This study tracks the long-term healing, remodeling, heterotopic bone formation and tumorigenesis during the segmental bone repair mediated by genetically engineered adipose-derived stem cells, and demonstrates the efficacy and safety of the therapy.

[1]Department of Chemical Engineering, National Tsing Hua University, Hsinchu, Taiwan.
[2]College of Medicine, Chang Gung University, Taoyuan, Taiwan.
[3]Department of Orthopaedic Surgery, Chang Gung Memorial Hospital, Taoyuan, Taiwan.
[4]Department of Nuclear Medicine and Molecular Imaging Center, Chang Gung Memorial Hospital, Taoyuan, Taiwan.
[5]Department of Medical Imaging and Radiological Sciences, Chang Gung University, Taoyuan, Taiwan.
*These two authors contributed equally to this work.

factor (VEGF) enhances angiogenesis, osteogenesis, and ossification.[5] The osteoinductive and angiogenic effects of both growth factors have prompted the combined use of BMP2/VEGF in recent years to synergistically promote the healing of cranial,[6] ulnar,[7] tibial,[8] and femoral[9] bone defects.

Cell therapy in conjunction with gene therapy to continuously supply growth factor(s) has evolved to ameliorate bone repair.[10] Among the cell sources, bone-marrow-derived mesenchymal stem cells (BMSCs) have drawn initial attention as they can heal large segmental defects[11] and can be genetically modified to augment *in vivo* bone formation.[8,12] Recently, adipose-derived stem cells (ASCs) also gained popularity for tissue regeneration because ASCs are easy to isolate in large quantities through liposuction and resemble BMSCs with respect to growth, morphology, and ability to commit to osteogenic differentiation.[13] These attributes inspired the use of ASCs to repair calvarial[14,15] and femoral[16] bone defects.

Baculovirus (BV) is an insect virus in nature but effectively transduces various mammalian cells without appreciable signs of cytotoxicity and viral replication,[17,18] hence sparking growing interests to exploit BV vector for diverse applications, including gene therapy, cancer therapy, and tissue engineering.[19–21] Critically, BV transduces BMSCs and ASCs at efficiencies exceeding 95%[22–26] and transiently expresses transgenes due to the nonreplication nature, thereby rendering BV a promising vector for gene delivery into BMSCs and ASCs. In light of these properties, we constructed recombinant BV vectors encoding human *bmp2* (Bac-CB) and *vegf* (Bac-CV) genes.[27] The New Zealand White (NZW) rabbit BMSCs were separately transduced with Bac-CB and Bac-CV, mixed, loaded to polymeric scaffolds, and transiently expressed functional BMP2 and VEGF. Transplantation of the BV-engineered BMSCs/scaffold constructs into massive (10 mm in length) femoral defects in NZW rabbits promoted the angiogenesis and segmental bone healing.[27]

Despite the promise of ASCs, ASCs were recently unraveled to be inferior to BMSCs in their capability of *in vitro* osteogenesis[28] and *in vivo* bone healing.[29,30] To repair large, segmental bone defects using ASCs, we hypothesized that sustained BMP2/VEGF expression was necessary. However, BV vectors naturally mediate transient expression due to the nonreplication nature, which may restrict its applications to scenarios requiring long-term expression. Thus, we developed a dual-BV vector system[23] in which one BV expressed the FLP recombinase (BacFLP) while the other BV harbored the Frt sequences—flanking human BMP2 (Bac-FCBW) or VEGF (Bac-FCVW) expression cassette.[25] Cotransduction of ASCs with BacFLP/Bac-FCBW or BacFLP/Bac-FCVW gave rise to FLP/Frt-mediated gene cassette excision off the BV genome, formation of episomal DNA minicircle, and hence prolonged transgene (BMP2 and VEGF) expression *in vitro*.[25] Allotransplantation of ASCs transduced with the dual-hybrid BV vectors expressing BMP2/VEGF into the massive segmental defects at the mid-diaphysis of femora in NZW rabbits accelerated the healing and improved the bone quality and angiogenesis, as judged by the formation of bone callus on the surface, and increase of bone volume and mechanical strength.[25] However, the biomechanical properties of the regenerated bone were still inferior when compared with the intact femora.

In this study, we further monitored the bone healing to 8 months post-transplantation by microcomputed tomography (μCT) to gain insights into the interior of the grafts. We also examined the remodeling process and explored whether the grafts developed into functional living bones with improved biomechanical properties. For this novel hybrid BV system, examining the biological safety issue is crucial for future applications. Therefore, whether the hybrid-BV-engineered grafts triggered heterotopic ossification and tumorigenesis was also examined by X-ray and positron emission tomography/computed tomography (PET/CT), respectively.

Materials and Methods

BV vectors, cells, and construct preparation

To compare the bone healing mediated by transient and prolonged BMP2/VEGF expression, we used two sets of BV vectors. Bac-CB[31] and Bac-CV[27] were constructed to transiently express human BMP2 and VEGF, respectively, under the control of CMV-IE promoter (Supplementary Fig. S1; Supplementary Data are available online at www.liebertpub.com/tea). BacFLP expressed FLP[23] while hybrid vectors Bac-FCBW[25] and Bac-FCVW[25] accommodated the Frt-flanking human *bmp2* and *vegf165* expression cassettes, respectively (Supplementary Fig. S1). All BV vectors were constructed previously and were titered by end-point dilution method.

ASCs were harvested subcutaneously from the inguinal fat pads surrounding epididymis of NZW rabbits (3–4 months old) and cells of passage 3 through 5 were used for experiments as described previously.[25] Transduction with Bac-CB or Bac-CV at a multiplicity of infection (MOI) of 100 was performed in T-75 flasks for 4 h using $NaHCO_3$-free Dulbecco's modified Eagle's medium (DMEM) as the surrounding solution.[23] In parallel, ASCs cultured in T-75 flasks were transduced with BacFLP (MOI 100) first for 4 h and then transduced with Bac-FCBW or Bac-FCVW (MOI 100) for another 4 h.[25] For mock transduction, virus-free, fresh TNM-FH medium (Invitrogen) was mixed with $NaHCO_3$-free DMEM at a volumetric ratio of 1:4 and added to the cells, and cells were gently shaken on a rocking plate at room temperature for 4 h. Following transduction, the virus mixture was removed and the cells were cultured in complete medium containing 3 mM sodium butyrate (Sigma). After 12 h of incubation, the medium was replaced by normal complete medium (without osteogenic supplements and butyrate) and the ASCs were trypsinized at 1 day post-transduction.

ASCs transduced with Bac-CB or Bac-CV were mixed at a number ratio of 4:1, loaded to concentric cylindrical poly (L-*lactide*-co-*glycolide*) (PLGA) scaffolds (outer diameter = 7 mm, inner diameter = 2 mm, height = 5 mm; total cell number = 1.5×10^6), and designated as the S group. The cells transduced with BacFLP/Bac-FCBW and BacFLP/Bac-FCVW were mixed at a ratio of 4:1, loaded to PLGA scaffolds, and designated as the L group. Likewise, mock-transduced ASCs were loaded to PLGA scaffolds and designated as the Mock group. The ASCs/scaffold implants were placed in 5% CO_2 at 37°C for 2 h for cell adhesion and cultured overnight prior to transplantation.

Animal surgical procedures

All animal experiments were performed in compliance with the Guide for the Care and Use of Laboratory Animals (National Science Council, Taiwan) and approved by the National Tsing Hua University Institutional Animal Care and Use Committee. For animal surgery, 5-month-old NZW rabbits (weighing = 3–4 kg) purchased from Animal Health Research Institute were randomly grouped and anesthetized by intramuscular injection of Zoletil 50 (25 mg/kg body weight) and 2% Rompun® (0.15 mL/kg body weight). A 10-mm section at the mid-shaft of the left femur was osteotomized using an oscillating saw and the defect was filled with two identical ASCs/scaffold implants (i.e., 3×10^6 cells/animal) from the Mock, S, or L group. Following the 0.9% saline rinse, the osteotomized site was stabilized with a stainless plate (DC-Plate; Synthes) and then the deep muscle layer and skin were closed.

Radiography, PET/CT, and μCT

The X-ray images were taken with the animals in supine position and with the right limb abducted and externally rotated. All X-ray images were captured at a distance of 100 cm from the animal.

For oncogenic metabolic analysis, normal ($n = 2$) and L group ($n = 7$) animals were subjected to PET/CT scan at 8 months before sacrifice using ^{18}F-labeled fluorodeoxyglucose (^{18}F-FDG) as the radiotracer, a glucose analogue widely used in PET imaging to detect unknown primary tumors in clinical oncology studies.[32] Briefly, the rabbits were fasted for ≥ 2 h before the procedure, anesthetized with 3% isoflurane, and received 3 mCi of FDG intravenously over 2 min. After a 45-min equilibration period during which the rabbits were at rest, the animals were positioned in the PET/CT scanner (Biograph 40 mCT; Siemens). The CT images were acquired with tube voltage of 120 KeV, pitch of 1.5, tube current of 20 mA, and exposure time of 500 ms. The axial scanning range was set as 50 cm with the abdomen at the center field of view and the CT images were reconstructed with the matrix size of $512 \times 512 \times 226$ and voxel size of $0.1875 \times 0.1875 \times 0.6\,mm^3$. The PET images were then acquired in list mode for 10 min and reconstructed with high-definition 3D ordered subset expectation maximization algorithm (2 iterations, 21 subsets, filter 3 mm, and zoom 1.3). Reconstructed attenuation corrected images were viewed in the transaxial, coronal, and sagittal planes. The PET and corresponding CT images were displayed in PMOD software workstation for alignment and were retrieved from dorsum to abdomen at an interval of 2 cm to provide coronal views for comparison.

At 3 and 8 months, the rabbits were first anesthetized by intramuscular injection of Zoletil 50/Rompun and then sacrificed by injecting intravenously an overdose of 2% lidocaine HCl. The femora were explanted, fixed in 4% phosphate-buffered formalin solution, and scanned with a μCT imaging system (Bioscan). The helical μCT data were acquired using a high-resolution frame as setup in the system, with tube voltage of 55 KeV, pitch of 1.0, and 180 projections. The axial scanning range was set as 3 cm with the bone defect at the center field of view. The μCT images with the matrix size of $280 \times 280 \times 300$ and an isotropic voxel size of 0.1 mm were reconstructed. The 3D-surface-rendering images were generated using Avizo software (Visualization Science Group) with the segmentation threshold determined from pilot scans on several specimens. The μCT images were visualized using PMOD software package in three axes to provide middle image slices of the graft site precisely and were also analyzed using PMOD software in each volume of interest (VOI) to calculate the bone volume and bone density (averaged Hounsfield units [HUs] in the cylindrical VOI) within the defect.

Biomechanical testing

After μCT analyses, all femora were subjected to biomechanical testing. The proximal and distal ends of the femur specimens were embedded in polymethylmethacrylate blocks and mounted on a combined axial motion and torsional-testing jig that was attached to a material testing instrument (ElectroForce® 3510; Bose). The distal end of the specimen was rotated laterally at a constant deformation rate of 1.0°/s until bone failure occurred. The applied load and angular displacement curves were used to compute the energy to failure, maximum torque to failure, and torsional stiffness.

Histochemical staining

After biomechanical testing, all femora were refixed in neutral-buffered formalin, cut into small pieces, decalcified in 0.5 M EDTA (pH 8.0) for 7–10 days, paraffin-embedded, and sectioned (5-μm thickness). Serial sections closest to the defect center were harvested, floated in water bath at 40°C, placed on organosilane-coated silanized microscope slides, and baked at 37°C overnight. The sections were deparaffined in xylene and rehydrated in serial ethanol baths for hematoxylin and eosin (H&E) staining. To examine the bone turnover, the sections were deparaffined, rehydrated, and stained with alkaline phosphatase (ALP) and tartrate-resistant acid phosphatase (TRAP) following the manufacturer's instructions (Cat. No. MK300; Takara). To identify cartilage formation, the deparaffined sections were rehydrated and stained with 3% Alcian blue (in glacial acetic acid) for 30 min, followed by dehydration with 100% ethanol.

Besides H&E staining of femoral sections, the heart, liver, spleen, lung, and kidney were removed from all L group animals at 8 months. Each organ was randomly dissected into three parts in 1-cm thickness, fixed in neutral-buffered formalin, and one section (5 μm in thickness) was picked from 100 consecutive sections for H&E staining.

Statistical analysis

All quantitative data were analyzed using Student's *t*-test and are expressed in average values. $p < 0.05$ was considered significant.

Results

Healing of segmental femoral defects as monitored by μCT

For animal experiments, three groups of constructs (Mock, S, and L groups, see Supplementary Table S1) consisting of cylindrical PLGA scaffolds and NZW rabbit ASCs were fabricated as described.[25] ASCs in the L group

were transduced with BacFLP/Bac-FCBW or BacFLP/Bac-FCVW for long-term expression (Supplementary Fig. S1) and mixed and seeded to the scaffold, while ASCs in the S group were transduced with Bac-CB or Bac-CV for short-term expression and mixed and seeded to the scaffold. The Mock group encompassed the mock-transduced ASCs. The cell/scaffold constructs were allotransplanted into the segmental bone defects (10 mm in length) at the mid-diaphysis of left femora of NZW rabbits (12 animals for the Mock group, 14 animals for the S group, and 14 animals for the L group). Serum samples were taken from some animals at different time points for the measurement of BMP2 and VEGF. Half of the animals were sacrificed at 3 months post-transplantation (3M), and the other half of the animals were sacrificed at 8 months post-transplantation (8M).

ELISA analyses showed that the Mock group imparted no enforced BMP2/VEGF expression while the S group mediated transient BMP2/VEGF expression that culminated at 3 days post-transplantation (dpt) and ceased after 7–14 days (Supplementary Fig. S2). In contrast, the L group conferred significantly higher and sustained BMP2 levels in the serum, which peaked (= 5.7 ng/mL) at 7 dpt and remained > 3.1 ng/mL for 28 days until returning to baseline levels at 56 dpt. The VEGF levels in the L group were also higher and more persistent than in the S group, peaking at 7 dpt (= 69.9 pg/mL) and remaining higher than background levels for 14 days (Supplementary Fig. S2).

To evaluate the bone healing, the femora harvested from the animals sacrificed at 3M and 8M ($n=6$ for the Mock group, $n=7$ for the S group, and $n=7$ for the L group for both time points) were first subjected to μCT. The 3D-surface-rendering μCT images (Fig. 1A) revealed that, without BMP2/VEGF overexpression, all animals in the Mock group failed to form apparent bone callus to bridge the gaps at 3M and 8M. The transient BMP2/VEGF expression in the S group slightly improved the bone repair,

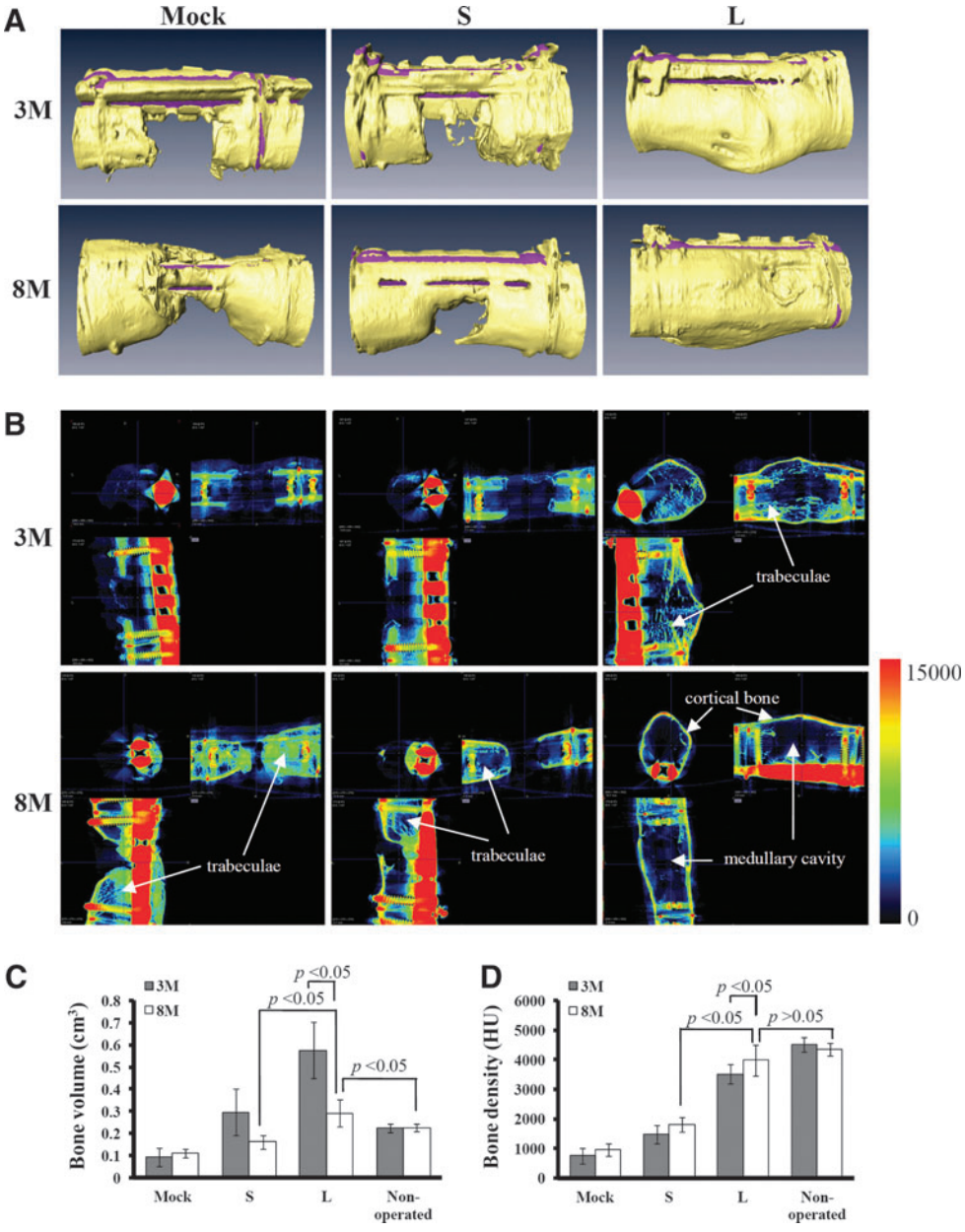

FIG. 1. Bone regeneration and remodeling as evaluated by microcomputed tomography (μCT) imaging. **(A)** Three-dimensional surface rendering images. **(B)** Transverses of μCT scans in *x*, *y*, and *z* axes. **(C)** Mean bone volume. **(D)** Mean bone density. The cell/scaffold constructs were allotransplanted into the segmental bone defects (10 mm in length) at the mid-diaphysis of femora of New Zealand White (NZW) rabbits (12 animals for the Mock group, 14 animals for the S group, and 14 animals for the L group). Half of the animals (six for the Mock group, seven for the S group, and seven for the L group) were sacrificed at 3M. The other half of the animals were sacrificed at 8M. That is, $n=6$, 7, and 7 for the Mock, S, and L groups (at both 3M and 8M), respectively. All femora were explanted and scanned with a μCT imaging system. The bone volume and bone density were calculated from the μCT data. The mean bone density represents the averaged Hounsfield units (HUs) in the cylindrical volume of interests (VOIs) of the regenerated bone. Color images available online at www.liebertpub.com/tea

resulting in callus formation and defect union in one rabbit at 3M and 8M (data not shown). However, the remaining animals only produced sparse bones in the gaps at 3M, and still failed to unite the defects at 8M (Fig. 1A). Strikingly, all animals in the L group led to callus formation and bone reunion at 3M ($n=7$), and exhibited signs of remodeling at 8M ($n=7$) as judged from the reshaping of callus (Fig. 1A).

The interior of the defect was elucidated by transverse μCT images in x, y, and z directions (Fig. 1B). The representative images of the Mock group confirmed that bone formation barely occurred inside the defect at 3M. At 8M trabecular bones developed within the defect but also wrapped the bony front, which could impede subsequent bone union. In the S group, the ingrowth of bony fronts was observed at 3M but bone formation in the interior remained scarce. At 8M, the bony fronts still failed to bridge the defect although some trabecular bones were observed. For all animals in the L group, the callus had connected both ends of the diaphyseal defect and trabecular network filled the interior at 3M. At 8M, bone collar was evidently formed and the interior trabecular network was resorbed and replaced by medullary cavity. The remaining trabeculae primarily lined the cortical bone on the periphery.

Based on the μCT data, the L group resulted in significantly higher bone volume (Fig. 1C) and bone density (Fig. 1D) than the Mock and S groups either at 3M or 8M (Supplementary Tables S2 and S3), again attesting the superior bone regeneration of the L group. Of note, the bone volume of the L group decreased from $=0.575\pm0.127\,cm^3$ (256%±57% of total defect volume) at 3M to $=0.292\pm0.063\,cm^3$ (129%±28% of total defect volume) at 8M, due to the resorption of trabecular bones and the reshaping of callus. The bone volume and bone density of the L group at 8M approached those of the nonoperated femoral bone (Supplementary Tables S2 and S3).

Bone reconstruction and remodeling as confirmed by histology

Natural diaphysis is composed of cortical bone, which surrounds a central medullary cavity containing bone marrow and adipose tissue. To evaluate the bone reconstruction, the femora harvested from the animals as shown in Figure 1 were sectioned and subjected to H&E staining. The H&E staining of the mid-diaphysis sections (Fig. 2) revealed that the middle of the Mock and S group grafts was mainly occupied by fibrous tissues at 3M and 8M, although some tiny bone islands were dispersed around the fibrous tissues in the S group. In sharp contrast, the L group was already filled with trabecular bone in the center of the defect at 3M ($n=7$), which was replaced by the fat-rich medullary cavity at 8M ($n=7$). Further, cortical bone with lamellar structures and blood vessels was clearly observed at 8M, indicating superior bone healing, remodeling, and vasculature reconstruction.

Bone remodeling necessitates orchestrated activities of osteoblasts (for bone formation) and osteoclasts (for bone resorption). To confirm the progression of bone remodeling, the center of regenerated bones at 3M and 8M was evaluated by histochemical staining (Fig. 3A) for ALP (an enzyme secreted by osteoblasts upon mineralization[33]) and TRAP (an enzyme marker for osteoclasts). The histomorphometric analyses of the staining data are shown in Supplementary Table S4. The barely detectable TRAP (arrows) and ALP (arrowheads) signals in the Mock group at 3M and 8M indicated very low osteoblast and osteoclast activities and a lack of bone turnover (Supplementary Table S4). In the S group, the ALP activity was negligible and only sparse TRAP signals were detected from 3M ($n=7$) to 8M ($n=7$), indicating that short-term BMP2/VEGF expression was unable to trigger effective mineralization and bone resorption. In the L group, abundant TRAP and ALP signals were observed at 3M ($n=7$), suggesting active bone resorption and mineralization (i.e., bone remodeling). At 8M ($n=7$) the ALP signals disappeared and only some TRAP signals remained detectable, indicating the waning of bone turnover activities.

Endochondral ossification, which commences from cartilage formation and is followed by chondrocyte hypertrophy and ossification, is a primary pathway for femur growth. Whether the bone healing proceeded via this pathway was examined by staining the mid-graft slices with Alcian blue

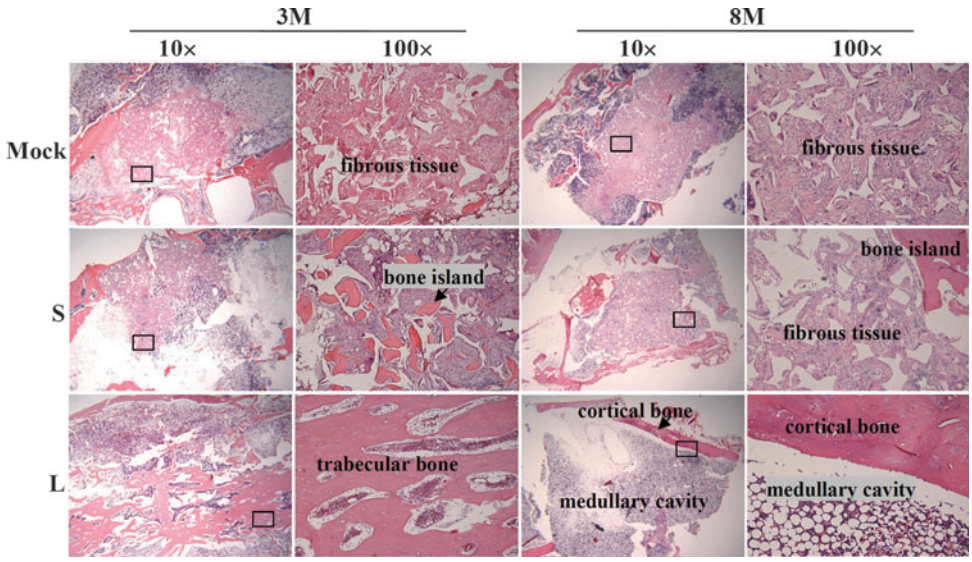

FIG. 2. Bone remodeling as confirmed by hematoxylin and eosin (H&E) staining. The mid-shaft of femora harvested at 3M and 8M as in Figure 1 were formalin-fixed, decalcified, paraffin-embedded, and sectioned (5-μm thickness) for H&E staining. $n=6$, 7, and 7 for the Mock, S, and L groups (at both 3M and 8M), respectively. Color images available online at www.liebertpub.com/tea

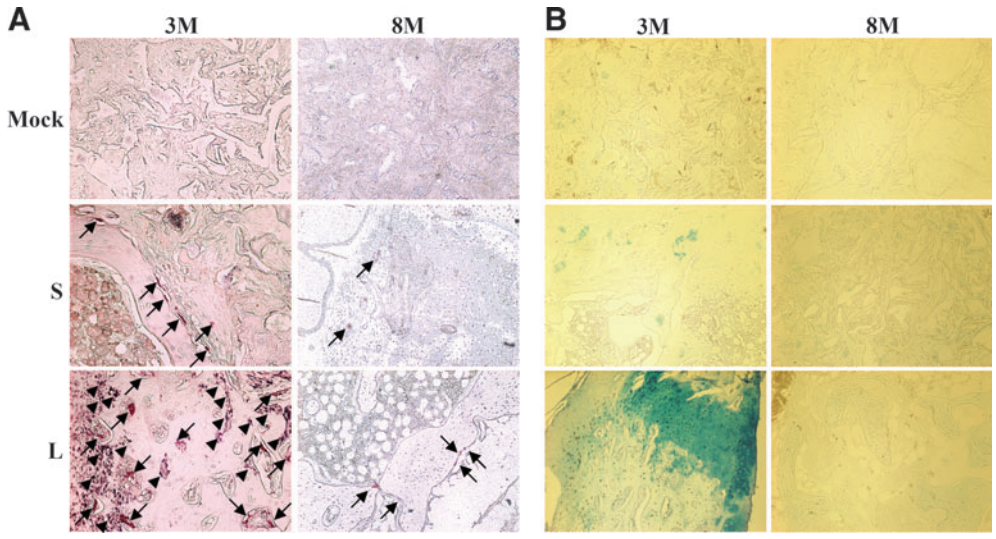

FIG. 3. Bone remodeling and bone formation pathway as confirmed by histochemical staining. **(A)** Tartrate-resistant acid phosphatase (TRAP)/alkaline phosphatase (ALP) staining. **(B)** Alcian blue staining. The mid-shaft of femora harvested at 3M and 8M as in Figure 1 were sectioned and stained for TRAP and ALP. In parallel, the slices were stained with Alcian blue to identify cartilage formation. Arrows indicate TRAP signals while arrowheads indicate ALP signals. $n=6$, 7, and 7 for the Mock, S, and L groups (at both 3M and 8M), respectively. Color images available online at www.liebertpub.com/tea

to indentify cartilage formation and subsequent histomorphometric analysis. Figure 3B and Supplementary Table S4 reveal only slight signs of cartilage formation in the Mock and S groups at 3M and 8M, which was consistent with the poor bone formation in these two groups. Conversely, cartilage formation was evident in the L group at 3M but disappeared at 8M, indicating active bone formation at 3M via the endochondral ossification, which ceased at 8M.

Biomechanical properties of regenerated bones

Whether the regenerated bones were biomechanically durable was evaluated by measuring the maximum torque (Fig. 4A), stiffness (Fig. 4B), and energy to failure (Fig. 4C) of the regenerated bones and nonoperated bones (as controls, $n=8$). Consistent with the μCT data (Fig. 1), the L group ($n=7$) gave statistically higher ($p<0.05$) maximum torque and stiffness than the S ($n=7$) and Mock ($n=6$) groups at 3M and 8M. Notably, the energy to failure, maximum torque, and stiffness of the L group at 8M were statistically comparable to those of the nonoperated femora ($p>0.05$), demonstrating that the healing and remodeling processes through 8 months conferred the L group femora sufficient biomechanical strength.

Absence of heterotopic bone formation and tumor formation

It was documented that supraphysiologic and sustained BMP2 expression would create a niche for adventitious heterotopic bone formation.[34,35] The representative X-ray radiographs (Fig. 5) attested that none of the Mock, S, and L group animals developed heterotopic bones, either at 3M or 8M.

To assess whether the BV-engineered ASCs gave rise to tumor formation, the normal rabbit (Fig. 6A, $n=2$) and all L group (Fig. 6B, $n=7$) animals at 8M were subjected to PET/CT scan. Representative coronal sections of CT (Fig. 6a) and PET (Fig. 6b) images were aligned side by side at the same levels, and the maximum intensity projections of both modalities were demonstrated for overview purpose (Fig. 6c, d). The rainbow-color scale for PET scan represents the amount of radiotracer uptake per tissue and no definite

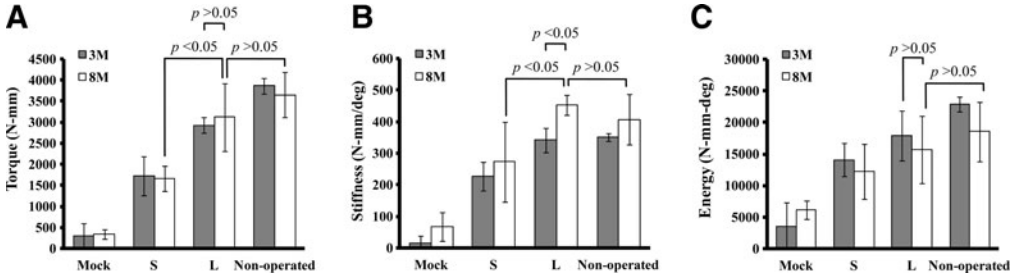

FIG. 4. Biomechanical properties of the femora harvested at 3M and 8M. **(A)** Maximum torque to failure. **(B)** Torsional stiffness. **(C)** Energy to failure. The femora harvested at 3M and 8M as in Figure 1 were subjected to biomechanical testing. The nonoperated femora taken from the contralateral limb served as the controls ($n=8$). $n=6$, 7, and 7 for the Mock, S, and L groups (at both 3M and 8M), respectively.

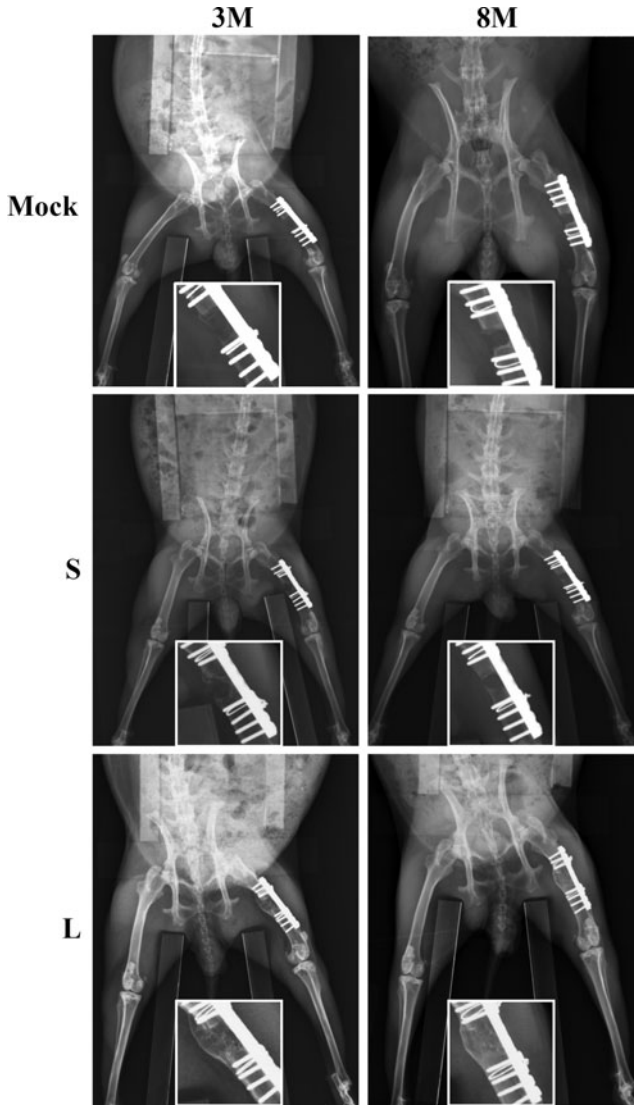

FIG. 5. Heterotopic bone formation as detected by X-ray radiography. $n = 6$, 7, and 7 for the Mock, S, and L groups (at both 3M and 8M), respectively.

abnormal increased radiotracer lesion was found in all animals. Although substantial physiological radiotracer uptake in the brain, salivary tissue, muscles, heart, stomach, liver, skeleton, kidney, and urinary bladder makes it difficult to differentiate normal and abnormal uptake, the PET and CT coregistration images revealed no detectable solid mass lesion in the solid organs, such as brain, liver, lung, and skeletons. Therefore, PET and CT scans collectively showed no abnormality in the whole-body survey, indicating the absence of tumor formation at gross levels. The PET/CT scans of other six rabbits in the L group similarly confirmed the absence of tumor formation (Supplementary Figs. S3–S8).

After sacrifice of the animals at 8M, the heart, liver, spleen, lung, and kidney were removed from the normal ($n = 2$) and L group animals ($n = 7$) and sectioned for H&E staining. The representative histopathological images demonstrated neither signs of malignant transformation nor distinguishable morphological differences between the normal and L group animals (Fig. 6C), attesting the absence of tumor formation in the L group animals at microscopic levels.

Discussion

Bone remodeling is a critical process that reshapes the bone tissues by removing, replacing, and reorganizing cells and matrix. Although a wealth of literature has reported the bone healing by genetically modified stem cells[36–40] and combined use of BMP2/VEGF to orchestrate bone healing has been demonstrated in recent years,[6–9] none of these studies has tracked the bone remodeling and evaluated potential side effects in a long term. Given the successful union of massive segmental bone defects mediated by hybrid BV-engineered ASCs/scaffold constructs, this study sought to monitor the bone remodeling and to assess the safety issues in a longer term. We attested that ASCs alone without ectopic BMP2/VEGF expression (Mock group) led to nonunion (Fig. 1) and the defect was still filled with fibrous tissues even at 8M (Fig. 2). Consequently, the Mock group was remarkably inferior to other groups in biomechanical properties. These data confirmed that ASCs alone were unable to heal such stringent bone defects and agreed with the poor bone regeneration by transplanting ASCs into large segmental bone defects.[41]

With transient BMP2/VEGF expression *in vivo* that culminated at 3 dpt (serum BMP2 = 1.5 ng/mL and VEGF = 34.4 pg/mL) and declined to baseline levels after day 14 (Supplementary Fig. S2), the S group slightly improved the bone formation, but still failed to unite the defect and was filled with fibrous tissues within the defect at 8M, despite vague signs of bone turnover at 3M (Supplementary Figs. S1–S3). As a result, the mechanical properties remained subpar when compared with the nonoperated femora (Fig. 4). Therefore, transient BMP2/VEGF expression mediated by ASCs was insufficient to heal such massive segmental defects even at 8M. This finding is contradictory to previous report that short-term BMP2 expression is sufficient to heal bone defect,[42] probably attributable to the disparity in the defect size, defect type, and cell source.

Strikingly, the L group mediated more robust and prolonged BMP2/VEGF expression (Supplementary Fig. S2) and concurrently led to bone reunion, trabecular bone formation via endochondral ossification in the interior, and bone remodeling at 3M, which proceeded with time and ultimately resulted in the resorption of trabecular bone (Figs. 1–3). The progression of remodeling gave rise to conspicuous reconstruction of medullary cavity and cortical bone with lamellar structure and vascularity at 8M (Figs. 1 and 2), and concomitantly ameliorated the mechanical properties that were comparable to those of contralateral, nonoperated femora (Fig. 4). It is known that a large diaphyseal defect that has been allografted can only be completely repaired if a cortex-to-cortex union is achieved and subsequent remodeling process progresses. However, vascularization and remodeling of cortical bone occur at a very slow rate.[43] The hybrid-BV-engineered ASCs/scaffold constructs not only healed and remodeled the massive segmental defects, but also revitalized the defects into living bone tissues with satisfactory strength in a manner

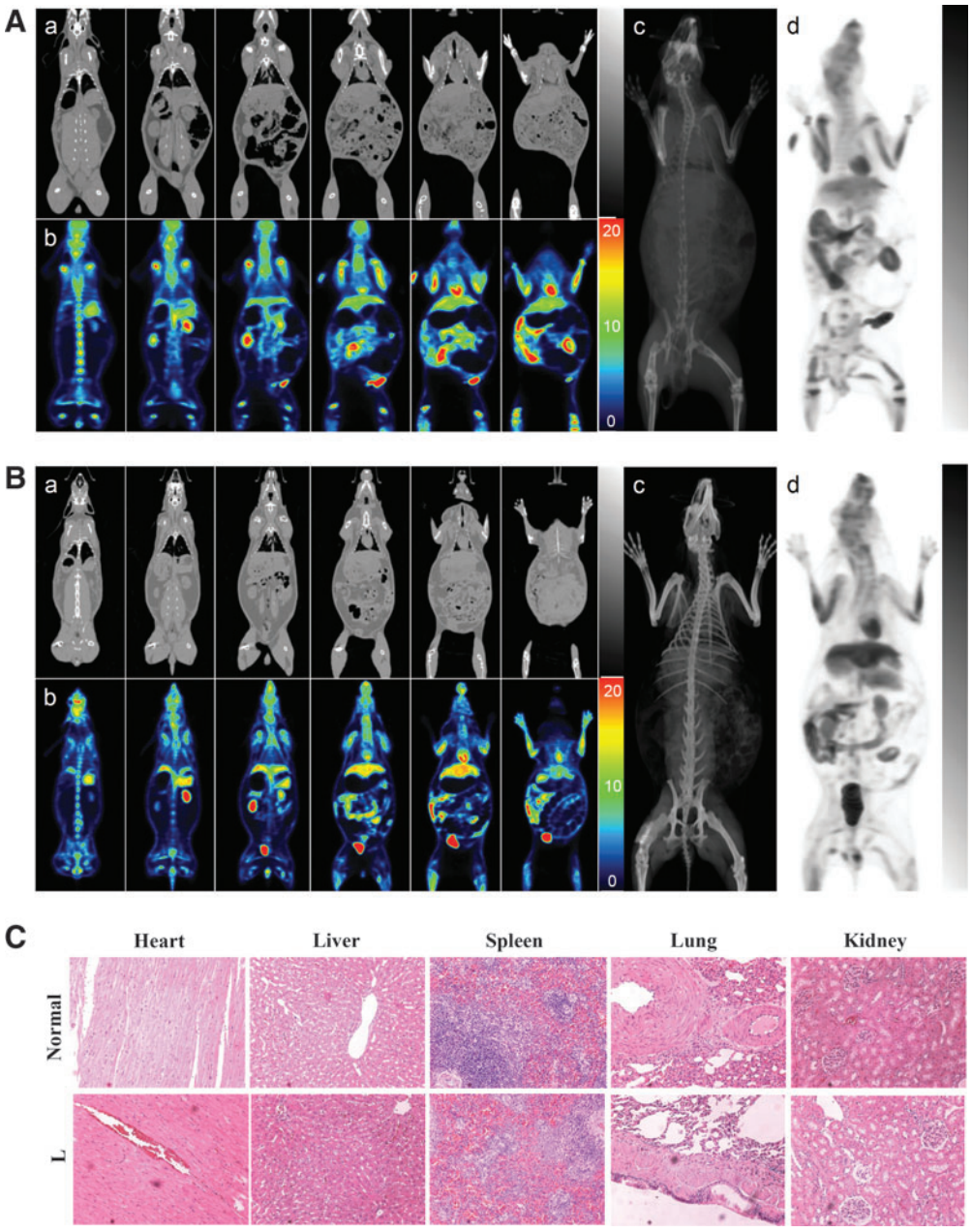

FIG. 6. Tumor formation as assessed by positron emission tomography/computed tomography (PET/CT) scans and histopathology. **(A)** PET/CT scan of a normal (nonoperated) rabbit. **(B)** Representative PET/CT scan of a rabbit in the L group at 8M. **(C)** H&E staining of sections from different tissues of the normal ($n=2$) and the L group animal ($n=7$). The subpanels in **(A, B)** are as follows: **(a)** CT coronal images, **(b)** PET coronal images, **(c)** projection of coronal CT images, and **(d)** projection of coronal PET images. The PET scan was performed using ^{18}F-labeled fluorodeoxyglucose (^{18}F-FDG) as radiotracer and each PET image slice was retrieved from dorsum to abdomen at an interval of 2 cm and aligned with the corresponding CT image. The whole-body PET and CT slices were projected onto 2D planar images. Color images available online at www.liebertpub.com/tea

mimicking the natural healing process, thus representing a remarkable advance in bone engineering.

It should be noted that the transplantation itself triggered pronounced inflammatory responses in the first week.[44] The inflammation subsided rapidly thereafter and was accompanied by cell apoptosis at 1 week post-transplantation and followed by complete eradication of transplanted cells after week 4.[44] These observations agreed with the notion that the transplanted stem cells often repair tissues by secreting growth factors without significant engraftment.[12] The findings, together with the significantly superior healing by the L group over the S group, underscore the importance of prolonged BMP2/VEGF expression in the healing and remodeling of such a massive, rigorous bone defect. The pivotal role of prolonged transgene expression supported the notion that a more sustained growth factor stimulation may be necessary to induce healing in more stringent bone repair scenarios.[38]

However, it should also be noted that BMSCs engineered with BV vectors for short-term BMP2/VEGF expression

successfully healed the massive segmental defects at the femora.[27] One may envisage that the transplanted cells were committed to osteogenic differentiation soon after transplantation under the influence of BMP2/VEGF, and acted in concert with the infiltrating host cells to fine-tune local microenvironments to promote bone formation and remodeling. As such, the beneficial roles of transplanted cells cannot be ruled out. Taken these parameters into account, the growth factor type, level, expression duration, and donor cell source are crucial for the repair. When BMSCs are used, transduction with BV vectors transiently expressing BMP2/VEGF is sufficient to heal the critical-size segmental bone defects. Conversely, when ASCs are employed, the hybrid BV vector mediating prolonged BMP2/VEGF expression is essential for the complete healing of such massive bone defects. Such high-level and prolonged BMP2 expression did not provoke local or remote heterotopic ossification in all seven rabbits (Fig. 5).

To date, sustained transgene expression is commonly achieved by viral vectors, such as adeno-associated virus (AAV), gammaretrovirus, and lentivirus.[45] However, the genotoxicity pertaining to the use of these viral vectors remains to be a roadblock to clinical applications. In particular, both gammaretrovirus[46] and lentivirus[47,48] integrate the transgene into the chromosome and have been reported to induce insertional transformation of hematopoietic cells and leukemia. AAV, despite existing in the transduced cells predominantly in the episomal form, may also integrate the transgene into the host chromosome[49] and trigger heptocellular carcinoma in mice.[50] Adenovirus is commonly used for bone engineering, yet adenovirus triggers potent immune response. Although gutless adenovirus vectors have been developed to reduce immune responses, the production and purification of gutless vectors remain challenging and costly.

In contrast to the aforementioned viral vectors, BV does not replicate in the transduced mammalian cells and the viral DNA is degraded over time,[20,51] which contributes to the transient expression nature. The hybrid BV vectors exploited the FLP/Frt-mediated recombination for circular episome formation, thereby reducing the chance of random integration. In fact, *in vitro* transduction of human BMSCs using the hybrid BV neither integrated the transgene into the chromosome and disrupted the karyotype of the BMSCs, nor elicited malignant transformation *in vitro*.[52] In this study, we further demonstrated that implantation of the hybrid-BV-transduced ASCs elicited no signs of tumorigenesis *in vivo* by histopathology and whole-body PET/CT (Fig. 6). Monitoring the tumorigenesis for a period of time longer than 8 months will further warrant the safety of the hybrid-BV-engineered stem cells for bone regeneration.

In conclusion, the constructs comprising ASCs engineered with the hybrid BV for sustained BMP2/VEGF expression induced reunion of the massive segmental bone defect, trabeculae formation at 3M, and triggered progressive bone remodeling and reconstruction of cortical bone and medullary cavity at 8M. Consequently, at 8M the regenerated bone tissue at the diaphysis structurally and biomechanically resembled the intact bone, without signs of heterotopic bone formation and tumorigenesis. These data collectively confirmed that the hybrid-BV-engineered ASCs and prolonged BMP2/VEGF expression are pivotal to revitalize the defect into the functional, living bone without appreciable side effects. Note, however, this hybrid vector relies on FLP expression and gene recombination within the cells. Excessive FLP expression within ASCs may compromise the cell viability; thus, optimal vector dose and transduction time should be carefully determined.

Acknowledgments

This work was supported by grants from the National Tsing Hua University (Toward World-Class University Project 102N2051E1), NTHU-CGMH Joint Research Program (101N2753E1, 102N2766E1, CMRPG3B0431, CMRPG390141, CMRPG300161, and CMRPG300131), CGMH Intramural Project (CMRPG300161, CMRPG391721, and CMRPG381001), and National Science Council (101-2628-E-007-009-MY3 and 101-2923-E-007-002-MY3), Taiwan.

Authors' Contributions

C.Y.L. performed experiments, analyzed data, and wrote the article. Y.H.C. performed analyses and wrote the article. L.Y.S., C.H.L., C.L.C., S.Y.L., and K.C.L. performed experiments. T.C.Y. performed analysis. K.J.L. performed experiments and wrote the article. Y.C.H. supervised the project and wrote the article.

Disclosure Statement

None of the authors declare competing interests.

References

1. Buckwalter, J.A., Einhorn, T.A., Bolander, M.E., and Cruess, R.L. Healing of the musculoskeletal tissues. In: Bucholz, R.W., Heckman, J.D., Court-Brown, C., Tornetta, P., Koval, K.J., and Wirth, M.A., eds. Rockwood and Green's Fractures in Adults. Philadelphia: Lippincott Williams & Wilkins, 1996, pp. 261–304.
2. Ross, M.H., Reith, E.J., and Romrell, L.J. Histology: A text and atlas. Baltimore: Williams & Wilkins, 1989.
3. Tseng, S.S., Lee, M.A., and Reddi, H. Nonunions and the potential of stem cells in fracture-healing. J Bone Joint Surg Am **90A,** 92, 2008.
4. Gamradt, S.C., and Lieberman, J.R. Genetic modification of stem cells to enhance bone repair. Ann Biomed Eng **32,** 136, 2004.
5. Peng, H., Usas, A., Olshanski, A., Ho, A.M., Gearhart, B., Cooper, G.M., and Huard, J. VEGF improves, whereas sFlt1 inhibits, BMP-2 induced bone formation and bone healing through modulation of angiogenesis. J Bone Mine Res **20,** 2017, 2005.
6. Young, S., Patel, Z.S., Kretlow, J.D., Murphy, M.B., Mountziaris, P.M., Baggett, L.S., Ueda, H., Tabata, Y., Jansen, J.A., Wong, M., and Mikos, A.G. Dose effect of dual delivery of vascular endothelial growth factor and bone morphogenetic protein-2 on bone regeneration in a rat critical-size defect model. Tissue Eng Part A **15,** 2347, 2009.
7. Geuze, R.E., Theyse, L.F., Kempen, D.H., Hazewinkel, H.A., Kraak, H.Y., Oner, F.C., Dhert, W.J., and Alblas, J. A differential effect of bone morphogenetic protein-2 and vascular endothelial growth factor release timing on osteogenesis at ectopic and orthotopic sites in a large-animal model. Tissue Eng Part A **18,** 2052, 2012.

8. Kumar, S., Wan, C., Ramaswamy, G., Clemens, T.L., and Ponnazhagan, S. Mesenchymal stem cells expressing osteogenic and angiogenic factors synergistically enhance bone formation in a mouse model of segmental bone defect. Mol Ther **18,** 1026, 2010.
9. Kempen, D.H.R., Lu, L., Heijink, A., Hefferan, T.E., Creemers, L.B., Maran, A., Yaszemski, M.J., and Dhert, W.J.A. Effect of local sequential VEGF and BMP-2 delivery on ectopic and orthotopic bone regeneration. Biomaterials **30,** 2816, 2009.
10. Evans, C.H., Ghivizzani, S.C., and Robbins, P.D. Orthopedic gene therapy in 2008. Mol Ther **17,** 231, 2009.
11. Reichert, J.C., Cipitria, A., Epari, D.R., Saifzadeh, S., Krishnakanth, P., Berner, A., Woodruff, M.A., Schell, H., Mehta, M., Schuetz, M.A., Duda, G.N., and Hutmacher, D.W. A tissue engineering solution for segmental defect regeneration in load-bearing long bones. Sci Transl Med **4,** 141ra93, 2012.
12. Prockop, D.J. Repair of tissues by adult stem/progenitor cells (MSCs): controversies, myths, and changing paradigms. Mol Ther **17,** 939, 2009.
13. Rada, T., Reis, R.L., and Gomes, M.E. Adipose tissue-derived stem cells and their application in bone and cartilage tissue engineering. Tissue Eng Part BRev **15,** 113, 2009.
14. Levi, B., James, A.W., Nelson, E.R., Vistnes, D., Wu, B., Lee, M., Gupta, A., and Longaker, M.T. Human adipose derived stromal cells heal critical size mouse calvarial defects. PLoS One **5,** e11177, 2010.
15. Cowan, C.M., Shi, Y.Y., Aalami, O.O., Chou, Y.F., Mari, C., Thomas, R., Quarto, N., Contag, C.H., Wu, B., and Longaker, M.T. Adipose-derived adult stromal cells heal critical-size mouse calvarial defects. Nat Biotechnol **22,** 560, 2004.
16. Lee, S.-J., Kang, S.-W., Do, H.-J., Han, I., Shin, D.A., Kim, J.-H., and Lee, S.-H. Enhancement of bone regeneration by gene delivery of BMP2/Runx2 bicistronic vector into adipose-derived stromal cells. Biomaterials **31,** 5652, 2010.
17. Abe, T., and Matsuura, Y. Host innate immune responses induced by baculovirus in mammals. Curr Gene Ther **10,** 226, 2010.
18. Kost, T.A., Condreay, J.P., and Ames, R.S. Baculovirus gene delivery: A flexible assay development tool. Curr Gene Ther **10,** 168, 2010.
19. Airenne, K.J., Hu, Y.-C., Kost, T.A., Smith, R.H., Kotin, R.M., Ono, C., Matsuura, Y., Wang, S., and Yla-Herttuala, S. Baculovirus: an insect-derived vector for diverse gene transfer applications. Mol Ther **21,** 739, 2013.
20. Chen, C.-Y., Lin, C.-Y., Chen, G.-Y., and Hu, Y.-C. Baculovirus as a gene delivery vector: Recent understandings of molecular alterations in transduced cells and latest applications. Biotechnol Adv **29,** 618, 2011.
21. Wang, S., and Balasundaram, G. Potential cancer gene therapy by baculoviral transduction. Curr Gene Ther **10,** 214, 2010.
22. Sung, L.Y., Chen, C.L., Lin, S.Y., Hwang, S.M., Lu, C.H., Li, K.C., Lan, A.S., and Hu, Y.C. Enhanced and prolonged baculovirus-mediated expression by incorporating recombinase system and in cis elements: a comparative study. Nucleic Acids Res **41,** e139, 2013.
23. Lo, W.-H., Hwang, S.-M., Chuang, C.-K., Chen, C.-Y., and Hu, Y.-C. Development of a hybrid baculoviral vector for sustained transgene expression. Mol Ther **17,** 658, 2009.
24. Lu, C.-H., Lin, K.-J., Chiu, H.-Y., Chen, C.-Y., Yen, T.-C., Hwang, S.-M., Chang, Y.-H., and Hu, Y.-C. Improved chondrogenesis and engineered cartilage formation from TGF-β3-expressing adipose-derived stem cells cultured in the rotating-shaft bioreactor. Tissue Eng. Part A **18,** 2114, 2012.
25. Lin, C.-Y., Lin, K.-J., Kao, C.-Y., Chen, M.-C., Yen, T.-Z., Lo, W.-H., Chang, Y.-H., and Hu, Y.-C. The role of adipose-derived stem cells engineered with the persistently expressing hybrid baculovirus in the healing of massive bone defects. Biomaterials **32,** 6505, 2011.
26. Lu, C.-H., Yeh, T.-S., Yeh, C.-L., Fang, Y.-H.D., Sung, L.-Y., Lin, S.-Y., Yen, T.-C., Chang, Y.-H., and Hu, Y.-C. Regenerating cartilages by engineered ASCs: prolonged TGF-β3/BMP-6 expression improved articular cartilage formation and restored zonal structure. Mol Ther **22,** 186, 2014.
27. Lin, C.-Y., Chang, Y.-H., Lin, K.-J., Yen, T.-Z., Tai, C.-L., Chen, C.-Y., Lo, W.-H., Hsiao, I.-T., and Hu, Y.-C. The healing of critical-sized femoral segmental bone defects in rabbits using baculovirus-engineered mesenchymal stem cells. Biomaterials **31,** 3222, 2010.
28. Im, G.I., Shin, Y.W., and Lee, K.B. Do adipose tissue-derived mesenchymal stem cells have the same osteogenic and chondrogenic potential as bone marrow-derived cells? Osteoarthritis Cartilage **13,** 845, 2005.
29. Niemeyer, P., Fechner, K., Milz, S., Richter, W., Suedkamp, N.P., Mehlhorn, A.T., Pearce, S., and Kasten, P. Comparison of mesenchymal stem cells from bone marrow and adipose tissue for bone regeneration in a critical size defect of the sheep tibia and the influence of platelet-rich plasma. Biomaterials **31,** 3572, 2010.
30. Lin, C.-Y., Chang, Y.-H., Kao, C.-Y., Lu, C.-H., Sung, L.-Y., Yen, T.-C., Lin, K.-J., and Hu, Y.-C. Augmented healing of critical-size calvarial defects by baculovirus-engineered MSCs that persistently express growth factors. Biomaterials **33,** 3682, 2012.
31. Sung, L.-Y., Lo, W.-H., Chiu, H.-Y., Chen, H.-C., Chuang, C.-K., Lee, H.-P., and Hu, Y.-C. Modulation of chondrocyte phenotype via baculovirus-mediated growth factor expression. Biomaterials **28,** 3437, 2007.
32. Delgado-Bolton, R.C., Fernandez-Perez, C., Gonzalez-Mate, A., and Carreras, J.L. Meta-analysis of the performance of ^{18}F-FDG PET in primary tumor detection in unknown primary tumors. J Nucl Med **44,** 1301, 2003.
33. Shegarfi, H., and Reikeras, O. Bone transplantation and immune response. J Orthop Surg **17,** 206, 2009.
34. Joseph, V., and Rampersaud, Y.R. Heterotopic bone formation with the use of rhBMP2 in posterior minimal access interbody fusion: a CT analysis. Spine (Phila Pa 1976) **32,** 2885, 2007.
35. Angle, S.R., Sena, K., Sumner, D.R., Virkus, W.W., and Virdi, A.S. Healing of rat femoral segmental defect with bone morphogenetic protein-2: a dose response study. J Musculoskelet Neuronal Interact **12,** 28, 2012.
36. Zou, D., Zhang, Z., He, J., Zhu, S., Wang, S., Zhang, W., Zhou, J., Xu, Y., Huang, Y., Wang, Y., Han, W., Zhou, Y., Wang, S., You, S., Jiang, X., and Huang, Y. Repairing critical-sized calvarial defects with BMSCs modified by a constitutively active form of hypoxia-inducible factor-1α and a phosphate cement scaffold. Biomaterials **32,** 9707, 2011.
37. Zou, D., Zhang, Z., He, J., Zhang, K., Ye, D., Han, W., Zhou, J., Wang, Y., Li, Q., Liu, X., Zhang, X., Wang, S., Hu, J., Zhu, C., Zhang, W., Zhou, Y., Fu, H., Huang, Y., and Jiang, X. Blood vessel formation in the tissue-

engineered bone with the constitutively active form of HIF-1α mediated BMSCs. Biomaterials **33,** 2097, 2012.
38. Virk, M.S., Conduah, A., Park, S.H., Liu, N., Sugiyama, O., Cuomo, A., Kang, C., and Lieberman, J.R. Influence of short-term adenoviral vector and prolonged lentiviral vector mediated bone morphogenetic protein-2 expression on the quality of bone repair in a rat femoral defect model. Bone **42,** 921, 2008.
39. Virk, M.S., Sugiyama, O., Park, S.H., Gambhir, S.S., Adams, D.J., Drissi, H., and Lieberman, J.R. ''Same Day'' *ex-vivo* regional gene therapy: a novel strategy to enhance bone repair. Mol Ther **19,** 960, 2011.
40. Zhu, L., Chuanchang, D., Wei, L., Yilin, C., and Jiasheng, D. Enhanced healing of goat femur-defect using BMP7 gene-modified BMSCs and load-bearing tissue-engineered bone. J Orthop Res **28,** 412, 2010.
41. Chou, Y.F., Zuk, P.A., Chang, T.L., Benhaim, P., and Wu, B.M. Adipose-derived stem cells and BMP2: Part 1. BMP2-treated adipose-derived stem cells do not improve repair of segmental femoral defects. Connect Tissue Res **52,** 109, 2011.
42. Noel, D., Gazit, D., Bouquet, C., Apparailly, F., Bony, C., Plence, P., Millet, V., Turgeman, G., Perricaudet, M., Sany, J., and Jorgensen, C. Short-term BMP-2 expression is sufficient for *in vivo* osteochondral differentiation of mesenchymal stem cells. Stem Cells **22,** 74, 2004.
43. Zhang, X.P., Xie, C., Lin, A.S.P., Ito, H., Awad, H., Lieberman, J.R., Rubery, P.T., Schwarz, E.M., O'Keefe, R.J., and Guldberg, R.E. Periosteal progenitor cell fate in segmental cortical bone graft transplantations: implications for functional tissue engineering. J Bone Miner Res **20,** 2124, 2005.
44. Lin, C.-Y., Lin, K.-J., Li, K.-C., Sung, L.-Y., Hsueh, S., Lu, C.-H., Chen, G.-Y., Chen, C.-L., Huang, S.-F., Yen, T.-C., Chang, Y.-H., and Hu, Y.-C. Immune responses during healing of massive segmental femoral bone defects mediated by hybrid baculovirus-engineered ASCs. Biomaterials **33,** 7422, 2012.
45. Thomas, C.E., Ehrhardt, A., and Kay, M.A. Progress and problems with the use of viral vectors for gene therapy. Nat Rev Genet **4,** 346, 2003.
46. Hacein-Bey-Abina, S., Von Kalle, C., Schmidt, M., McCcormack, M.P., Wulffraat, N., Leboulch, P., Lim, A., Osborne, C.S., Pawliuk, R., Morillon, E., Sorensen, R., Forster, A., Fraser, P., Cohen, J.I., de Saint Basile, G., Alexander, I., Wintergerst, U., Frebourg, T., Aurias, A., Stoppa-Lyonnet, D., Romana, S., Radford-Weiss, I., Gross, F., Valensi, F., Delabesse, E., Macintyre, E., Sigaux, F., Soulier, J., Leiva, L.E., Wissler, M., Prinz, C., Rabbitts, T.H., Le Deist, F., Fischer, A., and Cavazzana-Calvo, M. LMO2-associated clonal T cell proliferation in two patients after gene therapy for SCID-X1. Science **302,** 415, 2003.
47. Heckl, D., Schwarzer, A., Haemmerle, R., Steinemann, D., Rudolph, C., Skawran, B., Knoess, S., Krause, J., Li, Z., Schlegelberger, B., Baum, C., and Modlich, U. Lentiviral vector induced insertional haploinsufficiency of Ebf1 causes murine leukemia. Mol Ther **20,** 1187, 2012.
48. Modlich, U., Navarro, S., Zychlinski, D., Maetzig, T., Knoess, S., Brugman, M.H., Schambach, A., Charrier, S., Galy, A., Thrasher, A.J., Bueren, J., and Baum, C. Insertional transformation of hematopoietic cells by self-inactivating lentiviral and gammaretroviral vectors. Mol Ther **17,** 1919, 2009.
49. Nowrouzi, A., Penaud-Budloo, M., Kaeppel, C., Appelt, U., Le Guiner, C., Moullier, P., Kalle, C.v., Snyder, R.O., and Schmidt, M. Integration frequency and intermolecular recombination of rAAV vectors in non-human primate skeletal muscle and liver. Mol Ther **20,** 1177, 2012.
50. Donsante, A., Miller, D.G., Li, Y., Vogler, C., Brunt, E.M., Russell, D.W., and Sands, M.S. AAV vector integration sites in mouse hepatocellular carcinoma. Science **317,** 477, 2007.
51. Lin, C.-Y., Lu, C.-H., Luo, W.-Y., Chang, Y.-H., Sung, L.-Y., Chiu, H.-Y., and Hu, Y.-C. Baculovirus as a gene delivery vector for cartilage and bone tissue engineering. Curr Gene Ther **10,** 242, 2010.
52. Chen, C.-Y., Wu, H.-H., Chen, C.-P., Chern, S.-R., Hwang, S.-M., Huang, S.-F., Lo, W.-H., Chen, G.-Y., and Hu, Y.-C. Biosafety assessment of human mesenchymal stem cells engineered by hybrid baculovirus vectors. Mol Pharmaceut **8,** 1505, 2011.

Address correspondence to:
Yu-Chen Hu, PhD
Department of Chemical Engineering
National Tsing Hua University
101, Sec. 2, Kuang Fu Road
Hsinchu 300
Taiwan

E-mail: ychu@mx.nthu.edu.tw

Kun-Ju Lin, MD, PhD
Department of Nuclear Medicine
and Molecular Imaging Center
Chang Gung Memorial Hospital
Taoyuan 333
Taiwan

E-mail: lin4857@adm.cgmh.org.tw

Received: May 30, 2013
Accepted: December 2, 2013
Online Publication Date: April 22, 2014